

Modelling Horizontal Air Showers Induced by Cosmic Rays

M. Ave, R.A. Vázquez, and E. Zas

Departamento de Física de Partículas, Universidade de Santiago E-15706 Santiago de Compostela, Spain

Abstract

We present a framework for the study of muon density patterns on the ground due to showers produced in the atmosphere by cosmic rays incident at high zenith angles. As a checking procedure predictions of a model based on such a framework are compared to simulation results.

PACS number(s): 96.40.Pq; 96.40.Tv

Keywords:

I. INTRODUCTION

The old idea to detect neutrinos through Horizontal Air Showers (HAS) [1] has been recently brought to attention with the calculation of the acceptance of the Auger Observatories for the detection of high energy neutrinos [2]. At large zenith angles, cosmic rays (whether they are protons, heavier nuclei, or even photons) develop ordinary showers in the top layers of the atmosphere in a very similar fashion to the well understood vertical showers. Their electromagnetic component is however almost completely absorbed by the greatly enhanced atmospheric slant depth and prevented from reaching ground level. By contrast, high energy neutrinos may also induce Horizontal Air Showers (HAS) deeper into the atmosphere and hence resemble vertical air showers in their particle content at ground level, provided they interact sufficiently close to an air shower array.

The main background to neutrino induced HAS of very high energy (in the EeV range and above) is expected to be due to the remaining muon component of the cosmic ray

showers, after practically all the electromagnetic component is absorbed. A preliminary study of the air shower data at zenith angles above 60° from the Haverah Park array has shown that the observed rate is consistent to that expected from the ultra high energy ($E > 1$ EeV) cosmic rays arriving at large zenith angles [3]. These *muon showers* that penetrate the whole atmospheric slant depth to reach ground level are the object of this study which is intended to be detector independent. As the neutrino induced HAS rate that could be expected is quite low, zenith angle misreconstructions of vertical showers can also constitute a serious potential background to neutrino detection. However the relative importance of this background is very dependent on technical details of the experimental setup and, in particular, on the angular resolution actually achieved. Thus these matters cannot be further addressed in this article.

The interest in HAS induced by ordinary cosmic rays is not just limited to understanding the background of neutrino induced showers. The measurement of high zenith angle showers would enhance the aperture of existing air shower array data and it would increase the data on cosmic ray arrival directions to previously inaccessible directions in galactic coordinates [3]. Besides these obvious advantages, high zenith angle cosmic ray showers are unique because they select the muon component of the showers and they naturally probe a region of phase space which is quite inaccessible from vertical air shower measurements: the shower core.

The cosmic ray induced HAS are different mainly because they consist of muons which are produced far away from ground level. The particle density profiles for HAS induced by protons or heavy nuclei display complex muon patterns at the ground which result from the long path lengths travelled by the muons in the presence of the Earth's magnetic field [4,5]. These complex patterns are difficult to analyse [6] because the conventional approaches used for interpretation of low zenith angle showers ($< 60^\circ$) are usually based on the approximate circular symmetry of the density profiles. The analysis of HAS produced by cosmic rays requires a radically different approach.

Here we present a qualitative explanation of the ground muon patterns as well as ana-

lytical expressions for the muon density profile based on simple ideas. Our approach agrees remarkably well with simulation results for a wide range of distances to the core and zenith angles between 60° and 90° . Besides its convenience for data analysis which would otherwise depend on lengthy and cumbersome simulation results, the model gives a lot of insight into HAS and their complementarity to vertical showers and can be used for calculating the expected HAS rates for future detectors such as the Auger Observatories [7]. We also briefly discuss a simple method involving rotations for approximately generating muon ground density profiles for any azimuthal incidence using a single shower of the same zenith angle.

The article is organized as follows. In section II we present a toy model which describes the qualitative behavior of the ground muon patterns. In section III we discuss quite generally the implications of geomagnetic fields and the geometry implied. In section IV we extend the toy model to account for the magnetic field. In section V we give a detailed prescription to calculate muon densities for any azimuthal and zenith angle. In section VI we discussed the asymmetries that arise at ground level and introduce a number of ways to account for them. In section VII we compare the analytical densities obtained to those obtained with Monte Carlo simulations and finally in section VIII we summarize the achievements, briefly enumerating possible applications.

II. GENERALITIES: A TOY MODEL

The number of electrons, positrons and photons, the electromagnetic component, in an air shower induced by a 10^{19} eV proton rises as the shower penetrates higher depths to reach a maximum after which it rapidly becomes absorbed by low energy processes and the photoelectric effect. This component behaves much like shower size (number of electrons and positrons) reaching its maximum typically at $X_m = 750 \text{ g cm}^{-2}$. Below this depth it starts to become exponentially suppressed. The atmosphere is $\sim 1000 \text{ g cm}^{-2}$ deep for vertical showers doubling to $\sim 2000 \text{ g cm}^{-2}$ for 60° and becoming over 30 times deeper for completely HAS at sea level so that the electromagnetic component from π^0 decay can be

safely neglected at large zenith angles.

For inclined showers the main sources of electrons and photons at ground level are in fact the long range muons themselves, mainly through decay, but also through bremsstrahlung and pair production. The electron number density follows closely that of muons at all distances from shower axis and, as they are produced in small electromagnetic subshowers initiated by the decay electrons, their energy spectrum is very much like that expected in a vertical shower. A very similar argument applies to photons so that we can state that the total electromagnetic energy of an inclined shower is much less than the energy of the muonic component, unlike in vertical showers.

As the zenith angle rises, the average length traversed by the shower muons from their production point to the ground increases from ~ 10 km for vertical showers to ~ 300 km for nearly horizontal ones (see table I) . As a result only the muons produced with sufficiently high energy survive to ground level and this is crucial for HAS. Typically the energy loss ranges from a few GeV for the lowest energy muons in vertical showers to well over 100 GeV for a completely horizontal shower. As a result the average energy of the muons at ground level varies by close to two orders of magnitude between vertical and horizontal showers, as shown in table I.

We now introduce a very simple toy model that reproduces some of the qualitative features of the muon density patterns on the ground. Later we will build on this simple model to obtain parameterizations of muon densities at ground level. Let us consider a shower of zenith angle θ and assume that there is no magnetic field. At ground level we calculate muon number densities in a plane perpendicular to the shower axis: *the transverse plane*. In this plane the description of the shower becomes considerably simpler because it accurately respects the approximately cylindrical symmetry expected, except for minor effects due to changes in air density with height. This plane avoids the distortion of the muon densities resulting from the projection onto the Earth surface. Moreover, when the magnetic field is fully taken into account and the cylindrical symmetry is broken, as the azimuthal angle of the shower is rotated the muon density contours just rotate in the transverse plane

remaining otherwise practically unchanged as will be shown below.

We consider a highly relativistic muon of energy $E \simeq cp$, and transverse momentum p_{\perp} that travels a distance d to reach the ground. We assume this muon will only be deviated due to the p_{\perp} inherited from its parent pion (kaon) to arrive at distance r to shower axis in the transverse plane. This is equivalent to neglecting multiple scattering and deviations of the pions themselves from shower axis. In this case r is simply given by:

$$r = \frac{p_{\perp}}{p} d \simeq \frac{cp_{\perp}}{E} d. \quad (1)$$

This relation means that the muons of a given shower have distributions in E , d and p_{\perp} which are not independent.

For a given zenith θ the toy model is obtained taking an input energy distribution for the shower muons and fixing the values of d and p_{\perp} . The production distances d of the shower muons reaching ground level have a distribution fixed by shower development with an average $\langle d \rangle$ that rises as the zenith angle θ increases. As the development of inclined showers takes place in the upper layers of the atmosphere and spans only a small fraction of the atmosphere, the width of the d distribution is small compared to $\langle d \rangle$. This means that taking d to be a function of θ and ignoring its distribution can be a fairly good approximation. On the other hand the muon p_{\perp} results from multiple pion interactions in the shower development and has a relatively broad distribution. This is one of the reasons that prevents the toy model from being valid at quantitative level as will be shown below.

The virtue of this toy model is that it implies an approximately correct correlation between the muon energy, E , and its deviation from shower axis, r , through Eq. (1). Fig. 1 shows the correlation between the average muon energy and r as obtained in the simulation of one hundred 10^{19} eV proton showers without magnetic field effects. ¹ Such a relation means that at ground level the muon differential energy spectrum, $\phi[E] = dN/dE$, and the

¹This and all the simulations in this work, unless otherwise stated, have been generated with AIRES (version 1.4.2) [8] and SIBYLL (version 1.6) [9] for hadronic interactions.

number density, $\rho_\mu(r)$, are related through:

$$\rho_\mu(r) = -\frac{dE}{dr} \frac{1}{2\pi r} \phi[E(r)] = \frac{cp_\perp d}{2\pi r^3} \phi[E(r)]. \quad (2)$$

If for instance the energy spectrum of the shower muons is assumed to be $\phi(E) = AE^{-\gamma}$ the above relation implies:

$$\rho(r) = A \frac{(cp_\perp d)^{1-\gamma}}{2\pi} r^{-3+\gamma}. \quad (3)$$

In the absence of a geomagnetic field the toy model can be adjusted to roughly reproduce Monte Carlo results. One can use a muon energy spectrum $\phi[E] = dN/dE$ and d as obtained in simulations and only needs to adjust a single parameter namely p_\perp . We have done this exercise to obtain muon densities which are compared to AIRES simulations at different zenith angles. As an example Fig. 2 compares the results of simulation for three different zenith angles to density profile functions obtained with the toy model using the muon energy distributions from the simulations which are shown in Fig. 3. It is remarkable that such a crude model reproduces the muon lateral distributions to better than 30% in the interval $20 \text{ m} < r < 2 \text{ km}$ with a single p_\perp value of 200 MeV for all zenith angles considered. The results are nevertheless only academic since in practice the ground density profiles are severely modified by the Earth's magnetic field.

III. GENERALITIES: GEOMAGNETIC DEVIATIONS

To study the effect of the Earth's magnetic field we choose to decompose the field \vec{B} in two components \vec{B}_\parallel and \vec{B}_\perp , respectively parallel and perpendicular to shower axis. It is worth studying with a little detail the resulting geometry in the transverse plane since much of the ground pattern can be qualitatively understood in this way. We define two coordinate axes (x, y) in this plane, such that y is parallel to \vec{B}_\perp as shown in Fig. 4. In the transverse plane we define ψ as the angle between the y axis (or equivalently \vec{B}_\perp) and the direction parallel to the Earth's surface.

A muon travelling a distance d from the production site to the ground will bend its trajectory in a direction perpendicular to its velocity, \vec{v} and to \vec{B}'_{\perp} . Here \vec{B}'_{\perp} is the component of \vec{B} perpendicular to \vec{v} . If the muons are almost parallel to shower axis \vec{B}'_{\perp} largely coincides with \vec{B}_{\perp} and the transverse plane is perpendicular to the muon trajectory in this approximation. The parallel component of the Earth's magnetic field \vec{B}_{\parallel} can be neglected and neglecting other muon interactions and energy loss, the helicoidal trajectory is well approximated by an arc of a circle of radius R in the plane containing shower axis and \vec{B}_{\perp} .

For a complete description of the deviations we only need \vec{B}_{\perp} or, equivalently, its intensity B_{\perp} and the angle ψ . The circular symmetry of the shower in the absence of magnetic fields is distorted depending on the projected magnetic field B_{\perp} , the distance traversed by the muons, and their energy distribution. At low zenith the path length travelled is small and the circular patterns are hardly modified because the deviations are small. As the zenith rises the pattern turns first into an ellipsoid which eventually becomes two lobes at each side of B_{\perp} corresponding to the negative and positive charge muons deviating in opposite directions.

For a fixed zenith angle the density pattern in the transverse plane depends only on the intensity of the magnetic field. The pattern is oriented according to the direction of \vec{B}_{\perp} . Both the magnitude and direction of \vec{B}_{\perp} depend on the azimuthal angle of the shower ϕ . In this article azimuthal angles are measured counterclockwise with respect to the magnetic North. Figs. 5 and 6 respectively show how both these quantities vary as the azimuthal angle takes all possible values at two different locations, corresponding to Haverah Park [10] and Pampa Amarilla (the southern hemisphere Auger Observatory) [11] for illustrative purposes. On the basis of these two graphs alone and the discussion that follows it is straightforward to conclude that the muon density patterns in these sites will be completely different. A detailed study of HAS in Pampa Amarilla will be published elsewhere.

As the shower azimuthal angle varies at the Haverah Park site, B_{\perp} oscillates in magnitude about a central value. The oscillation amplitude decreases as the zenith angle rises being 15% (8%) of the central value for 70° (80°) zenith. It is remarkable that for this location once

the zenith angle θ is fixed at a high value, B_{\perp} is not too sensitive to the azimuthal direction of the shower ϕ . On the other hand as the zenith angle decreases the length transversed by the muons d becomes much smaller and the magnetic field is less effective in modifying the ground density profiles. While for low zenith the magnetic effect is small and there is little need for considering it, for high zenith B_{\perp} can be regarded as approximately independent of azimuth.

This means that we can make use of the fact that B_{\perp} is approximately azimuth independent to quickly generate HAS from a single simulation. If we fix the zenith angle to a high value, we make the approximation that B_{\perp} is constant and let the azimuth angle vary, the variations of the shower densities at ground level are only due to the corresponding changes in the angle ψ . In this approximation different azimuths are equivalent to a pattern rotation in the transverse plane. This approximation has important practical implications as it means that, given the zenith angle, a single shower can be used to generate muon density profiles on the ground for all azimuthal angles with the appropriate rotations of \vec{B}_{\perp} and projections onto the plane corresponding to the Earth's surface. This alone represents an important tool that can help the analysis of high energy HAS and has already been successfully used in the analysis of Haverah Park data presented in [3].

We have tested this economical means for generating HAS in a very simple fashion. We have generated approximate showers of predetermined azimuths from the results of a single shower. The ground level muon number density contours obtained in this way have been compared with the results of a direct simulations for the corresponding rotated azimuths. For the Haverah Park site as an example we have obtained approximate proton showers at $\phi = 90^{\circ}$ and 180° from the Monte Carlo results of a shower at $\phi = 0^{\circ}$ for three different zenith angles: $\theta = 60^{\circ}, 70^{\circ}, 80^{\circ}$. The rotated showers agree rather well with simulation results. Indeed fluctuations from shower to shower and the uncertainties introduced by thinning are much larger than the error made in the constant B_{\perp} approximation. At extreme zeniths ($\sim 87^{\circ}$) however the separated lobes on the ground plane obtained with simulations are slightly asymmetric. Clearly rotation in the transverse plane and simple projection onto

the ground cannot generate these asymmetries. These asymmetries arise because at high zeniths most of the muon deviation is due to the magnetic field and linear projection becomes inadequate. They can be taken into account as will be further discussed in section VI.

IV. GEOMAGNETIC DEVIATIONS IN THE TOY MODEL

The distinction between the two parameters p_{\perp} and d made in section II is important for considering geomagnetic field effects separately. We quantify the magnetic deviation through δx , the distance between the intersections of the two muon trajectories with and without magnetic effects and the transverse plane as shown in Fig. 7. Note that the coordinates x, y are conveniently chosen in the perpendicular and parallel directions to \vec{B}_{\perp} .

The geomagnetic deviation of the muons is easily shown to be:

$$\delta x = R \left[1 - \sqrt{1 - \left(\frac{d}{R}\right)^2} \right] \simeq \frac{d^2}{2R} = \frac{eB_{\perp}d^2}{2p}, \quad (4)$$

where e is the electron charge, R is the radius of curvature, and p is the muon momentum and we have expanded brackets to first order in d/R . For δx less than 2 km we expect it to be valid at the 5% level at zenith 60° because the typical production distance $\langle d \rangle$ is 16 km. At higher zenith the approximation is excellent. When we combine the above relation with Eq. 1 we obtain the following expression:

$$\delta x = \frac{eB_{\perp}d^2}{2p} = \frac{0.15B_{\perp}d}{p_{\perp}} \bar{r} = \alpha \bar{r}, \quad (5)$$

where in the last equation B is to be expressed in Tesla, d in m and p_{\perp} in GeV.

Physically \bar{r} (given by Eq. 1) corresponds to the muon deviation in the transverse plane *in the absence of magnetic field*. When \bar{r} and δx are small compared to d we can add them as two dimensional vectors in this plane. We can gain some insight in this relation considering that all muons (that for $\vec{B} = 0$ would intersect the transverse plane at a distance \bar{r} to the shower axis) are further deviated by $\vec{B} \neq 0$ a distance proportional to \bar{r} in the direction perpendicular to \vec{B}_{\perp} as schematically shown in Fig. 7. The μ^+ and μ^- deviate in opposite

senses so that the projection of the geomagnetic field in the transverse plane introduces a kind of mirror symmetry axis. We expect that the symmetry will not be exact being modulated by the expected excess of μ^+ respect to μ^- in atmospheric showers [12].

The dimensionless parameter α measures the ratio of the two described components of the displacement in the transverse plane, that due to the transverse momentum and that due to the magnetic field. Technically we can obtain the muon number density in the transverse plane in this model making the transformation:

$$\begin{aligned} x &= \bar{x} + \alpha\sqrt{\bar{x}^2 + \bar{y}^2}, \\ y &= \bar{y}. \end{aligned} \tag{6}$$

Here the barred (unbarred) coordinates represent the position of the muon in the transverse plane in the absence (presence) of the Earth's magnetic field. The muon number density is then:

$$\rho(x, y) = \bar{\rho}(\bar{x}(x, y), \bar{y}(x, y)) \left[\frac{\partial(\bar{x}\bar{y})}{\partial(xy)} \right], \tag{7}$$

where $\bar{\rho}(\bar{x}, \bar{y})$ is the density at distance $\bar{r} = \sqrt{\bar{x}^2 + \bar{y}^2}$ in the case $\vec{B} = 0$ and the last factor in brackets is the Jacobian of the transformation. We have checked that the above equations reproduce the main features observed in the muon density profiles in the transverse plane with magnetic fields. The muon number densities at ground level can be obtained after an appropriate projection onto the plane of the Earth's surface.

The value of α is a measure of the importance of the magnetic field. For instance for vertical showers we can plausibly set the distance to production to $d \sim 4$ km, $B_{\perp} \sim 10$ μ T, and $p_{\perp} \sim 0.3$ GeV, which gives $\alpha \sim 0.02$; *i.e.* α is very small and the effect of the magnetic field is not very important for vertical showers. For horizontal showers, however, d can be as large as 300 km and $B_{\perp} \simeq 40$ μ T, making $\alpha \gg 1$. For large values of α we expect that the density profiles obtained with $\vec{B} = 0$ are strongly modified.

It can be shown that if $\alpha > 1$ all μ^+ and μ^- are confined to a region in the transverse plane limited by two straight lines as illustrated in Fig. 9. The figure has been obtained with Eq. 7, $\alpha = 3$ and using a standard parameterization for the lateral muon distribution:

$\rho(r) \propto r^{-0.5}(1+r/a)^{-5}$ with $a = 1.5$ km. This result is qualitatively very important because it implies that for large zenith angles we expect *void regions* or *shadows* in which no muons are expected. The angle subtended by these voids is dependent on the parameter α , physically on the zenith angle. The effect can be easily explained with a geometrical construction matching the textbook graph for explaining the Cherenkov effect, see Fig. 8. The existence of these shadows is indeed the case as observed in simulations (see next section) and can be used for distinguishing between HAS produced by protons or nuclei high in the atmosphere and those produced by deeply penetrating neutrinos. These results are only valid at a qualitative level and hence the actual function used for $\rho(r)$ is not relevant. Further steps are needed to transform the toy model into a valid parameterization as shown below.

V. MUON NUMBER DENSITIES IN HAS

One of the reasons that has diffculted the study of HAS in particle array experiments is their intricate density profiles and their azimuthal dependence. Experiments with good sensitivity to particles incident at high zenith angles such as the Haverah Park Array did not have data from many stations that allowed the study of these effects from the experimental data. From the discussion of the previous section it is clear that the expected asymmetries due to the geomagnetic field depend on the value of the projection of \vec{B} onto the transverse plane. This projection obviously differs depending on the location of the experiment. For the purpose of checking the validity of the parameterizations that we present here, we have selected as an example the field corresponding to the Haverah Park array site, which has a value of $48.5 \mu\text{T}$, declination of -7.61° and inclination of 68.4° .

Unfortunately the toy model presented in the previous section is not good enough for quantitative purposes. The actual situation is more complicated even when $\vec{B} = 0$ because the transverse position of the muon, \bar{r} , is affected by both multiple scattering and the transverse position of the parent pions. Nevertheless the simple relation provided by Eq. 1 manifests a true correlation between \bar{r} and E which can be easily checked through simulation.

Fig. 1 shows how the *average* muon energy, $\langle E \rangle$, is clearly inversely related to distance from the shower axis \bar{r} as obtained in AIRES simulated proton showers at zenith angles 60° , 70° and 80° . To a very good approximation $\bar{r} \propto \langle E \rangle^{-\beta}$ where $\beta \sim 1.1$. We will now show how a relatively simple extension of the toy model converts it into a quantitatively valid parameterization of the muon component in HAS induced by cosmic rays.

The quantitative model proposed still makes use of Eq. 1, keeping d constant but assuming that at a given \bar{r} there is an energy distribution. It is more convenient to work with the variable $\epsilon = \log_{10} E$. In this variable the correlation can be approximated:

$$\langle \epsilon \rangle = A - \gamma \log_{10} \bar{r}. \quad (8)$$

For all zenith angles above 60° γ ranges between 0.73 and 0.83 (see table II and Fig. 10). Simulations show that as the transverse distance to the shower axis (\bar{r}) increases the width of the ϵ distribution at fixed \bar{r} varies slowly as shown in Fig. 10, being typically ~ 0.4 at $\bar{r} = 1$ km.

We now consider a muon "spectral density" in the new variable ϵ which is taken to be:

$$\rho(\bar{r}, \epsilon) = P(\epsilon; \langle \epsilon \rangle, \sigma) \rho(\bar{r}), \quad (9)$$

where P is a distribution of mean $\langle \epsilon \rangle$ and standard deviation σ . The distribution is normalized to 1 so that $\rho(\bar{r})$ is recovered after integration in ϵ .

To obtain the muon number density in the presence of the magnetic field we now have to perform the same transformation:

$$\begin{aligned} x &= \bar{x} + \frac{eB_\perp d^2 c}{2E}, \\ y &= \bar{y}. \end{aligned} \quad (10)$$

Note that this only differs subtly from Eq. 6 as three variables are now involved, namely x , y and ϵ , and the energy E in the first equation is now *independent* of \bar{r} . The analogous expression to Eq. 7 for the muon number density becomes:

$$\rho(x, y) = \int d\epsilon P(\epsilon, \langle \epsilon \rangle, \sigma) \rho(\bar{r}), \quad (11)$$

where in this case \bar{r} is given by:

$$\bar{r} = \sqrt{\left(x - \frac{eB_{\perp}d^2c}{2E}\right)^2 + y^2}. \quad (12)$$

The advantage lies in the fact that effects ignored in the toy model, such as the pion transverse momentum, are taken into account through the energy distribution. Once an approximate but realistic ϵ distribution is considered at a fixed \bar{r} , the model transforms into a quite accurate parameterization of the muon number density profiles in the transverse plane. This is not too difficult to understand if we consider the density contours as described in the previous section. For large values of α , which imply a shadow effect, the geometrical construction of the previous section implies largely enhanced densities accumulated at the border line of the shadow regions. This enhancement corresponds to the shock front in our Cherenkov analogy. The sharp edge of the distribution is an artifact of the toy model approach which becomes blurred when the E distribution is taken into account. The shadow angles are radically altered, so that they are no longer easily related to the parameter α . Muon number densities are also significantly modified with respect to the toy model in the previous section.

Eq (11) requires just four inputs namely a distribution for ϵ , the effective distance to the production site d , the relation between the mean of the distribution and \bar{r} and finally the lateral distribution function of the muons in the transverse plane. We have obtained reasonable choices for the inputs from the results of 100 proton showers of energy 10^{19} eV generated with AIRES for each zenith angle. All of these simulations must be made in the absence of magnetic fields for this purpose. For the ϵ distribution we choose a Gaussian with mean given by Eq. 8 and a fixed intermediate value of $\sigma \sim 0.4$ which is accurate enough for our purposes. In table I the production distance d is shown for zenith angles 60° , 70° , 80° and 87° . The required parameters for the mean in Eq. 8 can be read in Table II. Lastly for the lateral distribution function we fit a function of the NKG type [13]:

$$\rho(\bar{r}) = N \bar{r}^{p_1} \left[1 + \frac{\bar{r}}{a}\right]^{p_2}, \quad (13)$$

to the simulated results. The results of the fits are shown in Fig. 11 and the corresponding parameters are included in Table III. To take energy loss into account in a simple fashion we can replace E at the transverse plane in Eq. 12 by the average energy along the muon path which is considered to start at distance d . The number densities can now be easily obtained with Eq. 11 what completes our model.

VI. GROUND PLANE EFFECTS

Our results have been designed for the transverse plane to retain the maximum symmetries of the problem. In the event of equal number of μ^+ and μ^- it is easy to see that muon distributions must have a very accurate mirror symmetry about the line defined by the transverse component of the magnetic field (see Fig. 7). Unfortunately a projection (extrapolation) from the transverse onto the ground plane or vice versa must be made to compare our results both with real data or with simulation. If we just make the obvious rectangular projection which only involves the cosine of the zenith angle, the results on the ground will keep the mirror symmetry.

At high zenith angles however the results of a simulation show some distortion of this mirror symmetry, see Fig. 12. Clearly half of transverse plane is "below" ground level which means that in a real situation the muons arrive to the ground before reaching the transverse plane while the other half is "above" so that the muons have to travel more atmosphere before hitting the surface of the Earth. One way of quantifying the asymmetry is through $\mu^+ \mu^-$ ratio shown in Fig. 13. The μ^+ and μ^- are completely separated into two lobes which in general arrive at different times to the ground. As expected this effect is largest when the angle ψ (see Fig. 4) is smallest (corresponding to azimuth $\phi = 90^\circ$) but disappears at $\psi = 90^\circ$ (when the shower is aligned with the magnetic North $\phi = 0^\circ$).

The asymmetry arises because of the different muon paths from the production point to ground level. The cumulative effects of all muon interactions (such as magnetic deflections and continuous energy loss) and decays depend on the muon path. As a result the

asymmetries have a markedly geometrical nature growing as the distance to shower core increases. This is fortunate since simple geometrical algorithms can be devised to correct these asymmetries when necessary.

The two sources of muon deviations from shower axis that have been considered in previous sections account for most of the geometric effect. For each zenith angle the muon paths are considered to start at a fixed distance d to the transverse plane. Corrected projections must take this common origin of the muon paths into account that clearly generates an asymmetry on the ground plane. The muon deviations due to the magnetic field are also a clear source of asymmetry, which is quadratic on the muon path (arcs of circle). When this is taken into account the simulated results can be "projected" onto the transverse plane in a way that most of the asymmetries arising at high zenith angles can be removed.

There are several possibilities available for projection, the easiest being the obvious rectangular projection. Such a projection is enough for most purposes because the asymmetries are small, except for extreme zenith angles. For such cases the "quadratic" deviation due to the magnetic field becomes most important and we have two ways to account for it depending on whether we work with simulated results or not. We can project simulated results onto the transverse plane just extrapolating the individual muon trajectories since all the information on the particles reaching the ground is easily available in a simulation. Alternatively one can use approximate geometrical projections which will be shown to be sufficiently accurate in spite of ignoring the details of the individual muons. This is because of the discussed correlation between energy and position of the muons.

Clearly individual muon extrapolation is the best way of obtaining the muon densities in the transverse plane. A simple helix would only neglect muon energy loss and decay and some correction can be further implemented to account them. For a purely geometrical extrapolation we will use the following procedure which is shown to be sufficient for all purposes. In the direction parallel to B_{\perp} one simply joins the muon position to the fixed production point while in the orthogonal direction one considers muon trajectories which are circles tangent to shower axis at the same production point. In Figs. 12 and in Fig. 13

the results of the rectangular projection are compared to the extrapolation of the simulated densities for a shower at extreme zenith $\theta = 87^\circ$ and having azimuth $\phi = 90^\circ$ (maximum asymmetry). A large fraction of the unwanted asymmetries in the transverse plane is equivalently removed with either of the two methods. The residual asymmetries are mostly due to muon decay and the neglect of muon energy loss. For distances to shower core below 4 km the residual asymmetry is below 20%; it should be stressed that this range corresponds to distances up to 80 km away from shower core in the ground plane.

In the analytical results obtained for the muon densities in the transverse plane (previous section) the information on the individual muon energy and direction is lost. Fortunately the geometrical algorithm to remove the asymmetries can be inverted to convert the symmetric results obtained in our model to the ground, approximately reproducing the asymmetries, what makes it appropriate for comparison with data to the precision level indicated by these graphs. The systematic error in the ground projection that would be generated at large r could be largely removed accounting for asymmetries due to energy loss and muon decay.

VII. RESULTS

Testing the muon number density results obtained with the prescription described in the previous section by comparison with dedicated simulations is by no means a straightforward task. The main difficulty arises from the uncertainties associated with the muon densities on the ground plane that are obtained with any simulation program which necessarily implies the statistical treatment of shower particles, *thinning algorithms*, for the energies considered to avoid excessive computing times. There is a complex combination of statistical fluctuations, shower fluctuations and thinning fluctuations which is rather difficult to unravel. The simulated muon number density results fluctuate depending on the two dimensional binning choices which are rather awkward to choose because of the complexity of the patterns involved particularly at the highest zenith angles.

For testing purposes, we choose to compare the densities obtained with the described

prescription to the results of simulations using AIRES [8] with the magnetic effects on. We have also generated 100 proton showers of energy 10^{19} eV and azimuths $\phi = 0^\circ$ and 90° for each zenith angle (60° , 70° , 80° , and 87°). We project the average muon densities (over the 100 showers) onto the transverse plane as described in the previous section to eliminate the asymmetries and to compare to the results of our model.

The number density results of Eq. (11) are compared to the averages obtained with the specific simulations made. No normalization has been made in the comparisons shown in Figs. 14–19 that illustrate the reach of our results. The figures shown very much speak on their own. The agreement is rather impressive considering the ranges of distances involved and particularly the ranges in densities which can span over four orders of magnitude. We firstly show in Figs. 14 and 15 two density contour plots for two different zeniths. These graphs display well defined shadow regions as anticipated and show an excellent agreement in the shape of the densities obtained compared to the simulation results. The isolated density spots in the simulation also indicate very clearly how the fluctuations due to the simulation become very important even at distances very close to shower axis in some specific directions. The figures even suggest that in many respects the parameterization results are "better behaved" in the sense that they avoid many unphysical fluctuations and can be extrapolated to very low muon densities.

Quantitative tests of the average two dimensional density distribution in polar coordinates integrated over the radial (azimuthal) coordinate up to 6 km (up to 2π) in the transverse plane are shown in Fig. 16 (Fig. 17). The bars are indicative of the statistical errors in the obtained averages taking into account shower fluctuations and poisson statistics. These graphs are particularly good for stressing systematic effects that are cumulative and highlight the discrepancies. The disagreement is largest for the highest values of r so that the highest discrepancies correspond to low muon number densities where results are going to be less relevant. As stressed before some of the differences between the model and the simulation are due to muon decay and are thus still an artifact of using results on the ground plane for comparison with our analytical muon number densities. They are never-

theless indicative of the uncertainties that can be expected if geometrical projections are used for obtaining densities at ground level ignoring muon decay. These are below statistical fluctuations and consequently quite hidden by shower fluctuations.

Lastly, Fig. 18 shows the x distribution calculated in a 40 meter bin centered at $y = 0$ while Fig. 19 shows the y distribution for a 40 meter bin centered at $x = 1$ km. Although for the highest zenith (87°) the r distributions disagree above the 20% level for r distances exceeding 4 km in the transverse plane, the discrepancies in the actual densities correspond to very low values of the densities which are relatively less important.

VIII. SUMMARY AND DISCUSSION

We have successfully obtained a framework for studying the muon content of HAS produced by protons in the atmosphere. It can be effectively considered as a semianalytical parameterization for the muon number densities in the transverse plane for HAS. Although it relies on Monte Carlo it can be considered as an alternative to it since the simulation is only needed in first instance to obtain the inputs ignoring the magnetic effects and hence eliminating azimuthal angle dependences. Although only proton showers of 10^{19} eV energy have been considered for the Haverah Park site, this framework is completely general and can be applied to showers of any energy and composition located in any site in a completely analogous fashion.

The method consists of splitting the muon propagation in a shower into two fictitious parts, one which takes place in the absence of a magnetic field and a second one in which the magnetic effects are separately analysed. As the first part preserves the approximate circular symmetry of the shower development it allows simple parameterizations in terms of a single variable. The second part can be implemented in an analytical way. As a spinoff we have obtained a way to obtain ground density profiles of fixed zenith angle but any azimuthal angle from a single shower of the corresponding zenith.

We expect to refine this model by improving the fits for the required inputs and including

ignored effects such as correlations between muon impact position and distance to production site, muon decay, and distributions of distance to production site. These ignored effects could be implemented in an analogous way to the introduction of the energy distribution. Although these refinements may be necessary in the future, we do not feel at this time there is need to be so accurate since there are many uncertainties in the simulation programs which surely exceed the precision level of the results obtained. The simulations used require extrapolations of cross sections and distributions of particle interactions in energy regions which are well above those explored in current particle physics experiments or those to be made in the near future.

Besides giving insight into the complexity of large zenith angle showers, the results presented here have a rather broad range of applications connected with the detection of Horizontal Air Showers. The need of systematic simulations of complicated high energy showers which is very time consuming can be avoided. Such a task is of great help for the analysis of large zenith angle data as well as for the study of the sensitivity of these air showers to any of the current concerns about the highest energy cosmic rays such as the expected acceptance of Pierre Auger Observatories [11].

Acknowledgements: We are indebted to A.A. Watson for having introduced us into the real experimental problems of HAS and an invitation to Leeds when most of this work was initially conceived. We also thank J.A. Hinton, G. Parente, and A.A. Watson for many discussions and also for comments after reading our manuscript. This work was partly supported by a joint grant from the British Council and the spanish Ministry of Education (HB1997-0175), by Xunta de Galicia (XUGA-20604A98) and by CICYT (AEN99-0589-C02-02).

REFERENCES

- [1] V.S. Berezinsky and A. Yu. Smirnov, *Astrophys. Space Science* **32** (1975) 461.
- [2] J. Capelle, J.W. Cronin, G. Parente, and E. Zas, *Astropart. Phys.* **8** (1998) 321.
- [3] M. Ave, R.A. Vázquez, E. Zas, J. Hinton, and A.A. Watson, *Proc. of the 26th ICRC*, Vol. 1, p. 365 (1999).
- [4] A.M. Hillas *et al.*, *Proc. of the 11th ICRC, Budapest (1969)*, *Acta Physica Academiae Scientiarum Hungaricae* 29, Suppl. 3, pp. 533-538, (1970). Lawrence, M.A., Reid, R.J.O., and Watson, A.A. (1991).
- [5] D. Andrews *et al.*, *Proc. of the 11th ICRC, Budapest (1969)*, *Acta Physica Academiae Scientiarum Hungaricae* 29, Suppl. 3, pp. 337-342, (1970).
- [6] E.E. Antonov, L.G. Dedenko, Yu.P. Pyt'ev *et al.*, *Pis'ma Zh. Éksp. Teor. Fiz.* **69** (1999) 614 (*JETP Letts.* **69** (1999) 650).
- [7] M. Ave, *PhD Thesis, in preparation* (2000)
- [8] J. Sciutto, *AIRES: A System for Air Shower Simulation*, GAP note 1998-005.
- [9] R.T. Fletcher, T.K. Gaisser, P. Lipari, and T. Stanev, *Phys. Rev.* **D50** (1994) 5710; J. Engel, T.K. Gaisser, P. Lipari, and T. Stanev, *Phys. Rev.* **D46** (1992) 5013.
- [10] M.A. Lawrence, R.J.O. Reid, and A.A. Watson, *J.Phys.* **G17** (1991) 733.
- [11] *The Pierre Auger Project Design Report*. By Auger Collaboration. FERMILAB-PUB-96-024, Jan 1996. 252pp.
- [12] W.R. Frazer *et al.*, *Phys Rev.* **D5** (1972) 1653.
- [13] K. Kamata and J. Nishimura, *Prog. Theor. Phys. (Kyoto) Suppl.* **6** (1958) 93.

TABLES

θ (degrees)	d (km)	Δd (km)	$\langle E \rangle$ (GeV)	ΔE (GeV)	$N_\mu \times 10^{-6}$	$\Delta N_\mu \times 10^{-6}$
0°	3.9	2.8	8.1	33.3	29.	6.5
60°	16	6.5	18.9	90	13.3	2.4
70°	32	10	32.9	208	7.8	1.4
80°	88	17	77	486	3.3	0.7
87°	276	31	204	1186	1.2	0.2

TABLE I. Relevant parameters for muon production as obtained in 100 proton showers of energy 10^{19} eV with a relative thinning of 10^{-6} simulated with AIRES using SIBYLL 1.6 cross sections. Average values and RMS deviations for production altitude (d), muon energy at production ($\langle E \rangle$), and total number of muons at ground level (N_μ).

θ (degrees)	γ	A
60°	0.75 ± 0.1	2.67 ± 0.23
70°	0.73 ± 0.06	4.04 ± 0.20
80°	0.81 ± 0.07	3.63 ± 0.20
87°	0.83 ± 0.07	4.15 ± 0.20

TABLE II. Best values for the parameters in the relation between average muon energy and distance to shower core (Eq. 8) and corresponding errors, as obtained in the fit to the simulated results.

θ (degrees)	N	p_1	p_2	a (m)
60°	569.9	-0.52	-4.05	782.8
70°	227.1	-0.49	-4.35	1010
80°	78.4	-0.52	-4.49	1513
87°	20.2	-0.51	-5.43	2171

TABLE III. Best values for the parameters in the lateral distribution function in Eq. 13 as obtained in a fit to the simulated results.

FIGURES

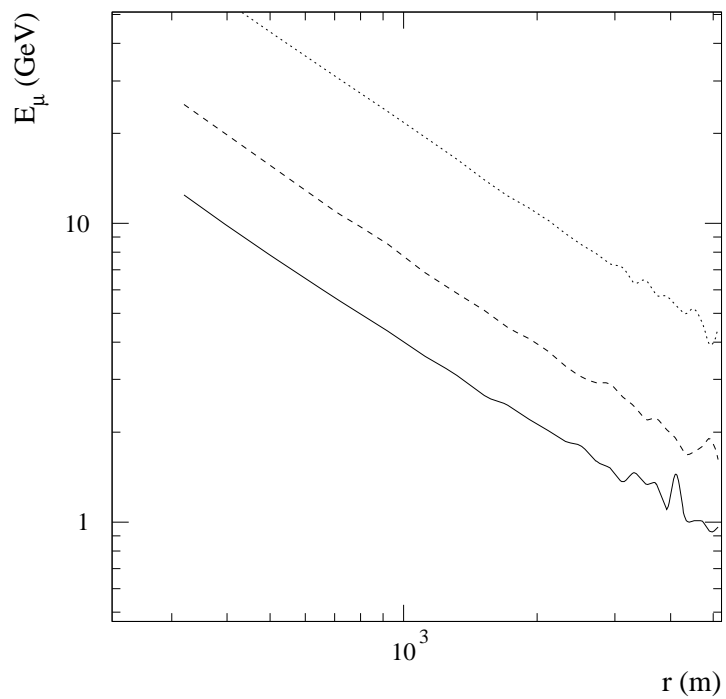


FIG. 1. Average muon energy as a function of distance to shower core. Results obtained with simulation using Aires for 10^{19} eV proton showers of zenith angle 60° , 70° , and 80° from bottom to top.

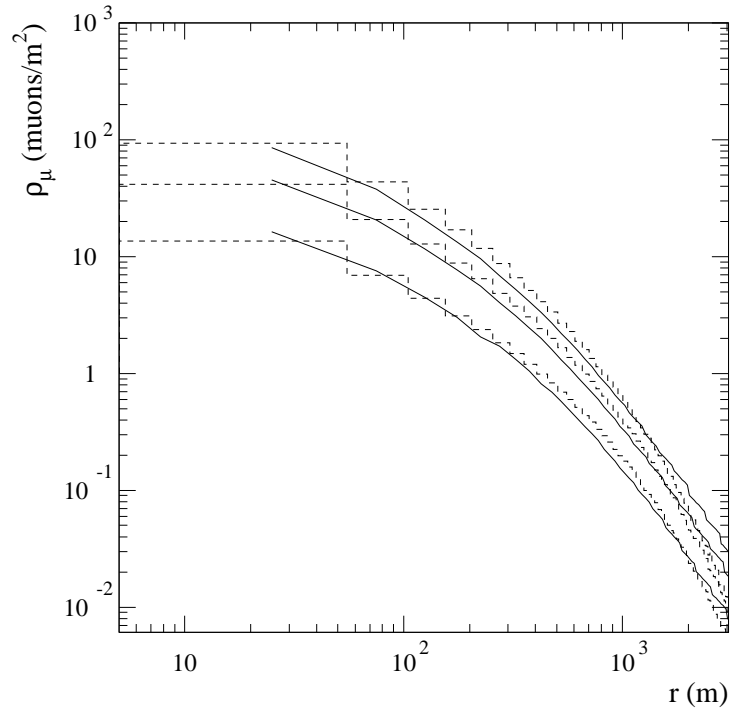


FIG. 2. Lateral distribution of muons as obtained in the toy model (continuous lines) and in the simulation (dashed lines). Figures correspond from top to bottom to zenith angles 60° , 70° , and 80° .

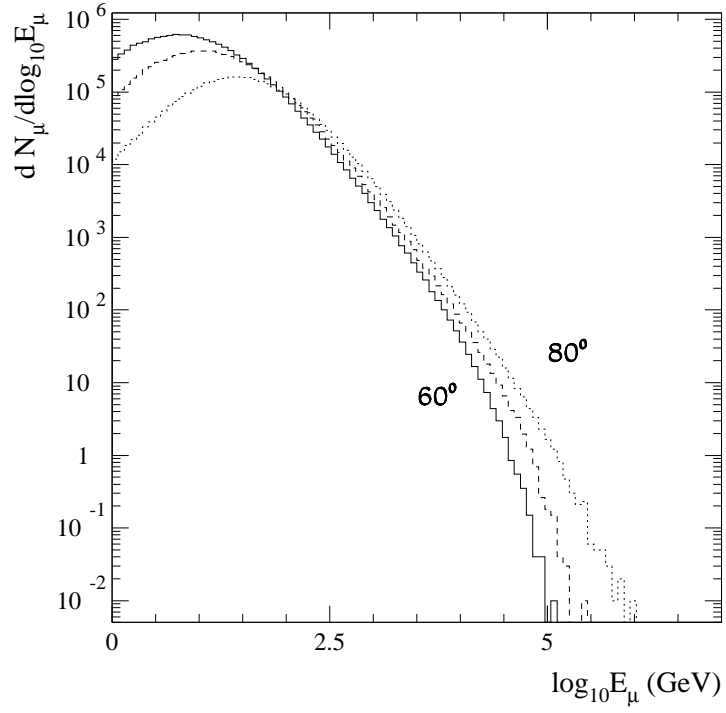


FIG. 3. Energy spectrum of muons at ground level for 10^{19} eV proton showers simulated with AIRES, for zenith angles 60° (full line), 70° (dashed line), and 80° (dotted line).

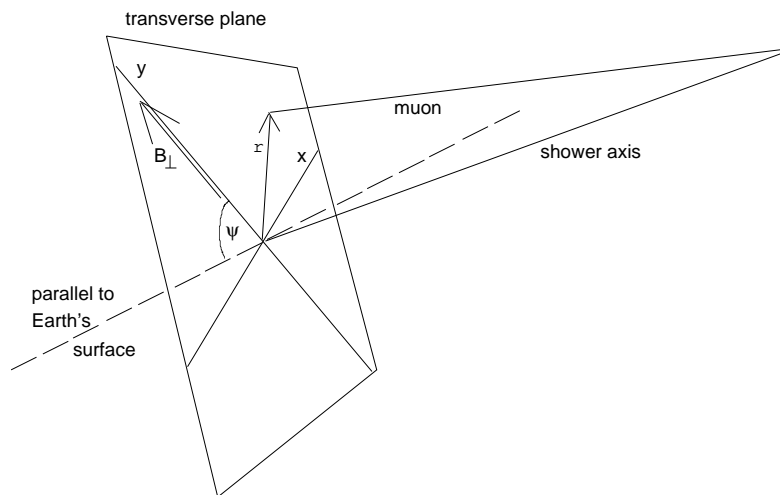


FIG. 4. The plane perpendicular to the shower axis or *transverse plane* and some useful geometrical definitions for Horizontal Air Showers. The y axis is chosen along the direction of B_{\perp} which is the projection of the magnetic field onto the transverse plane. ψ is the angle subtended by the y axis and the intersection of the transverse and the ground planes.

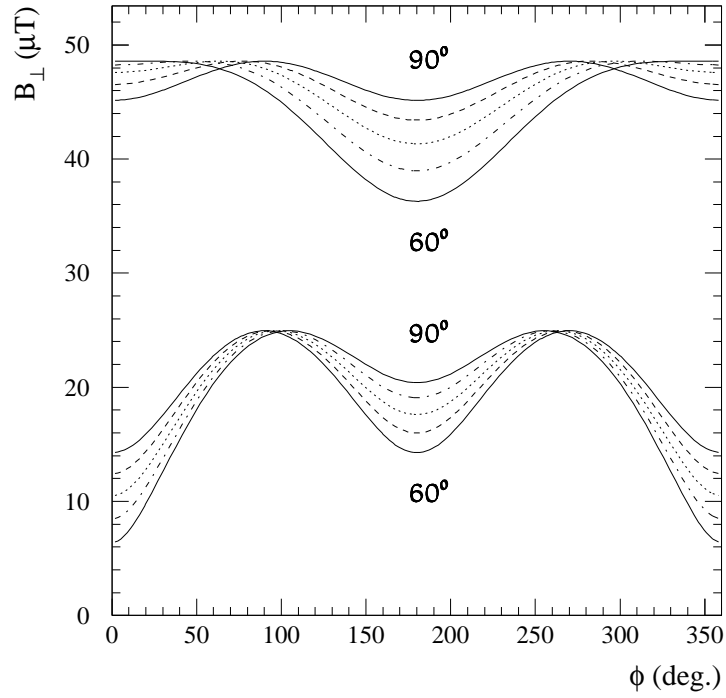


FIG. 5. Magnetic field projection onto the transverse plane as a function of azimuthal angle for the Haverah Park location (top lines) and Pampa Amarilla (bottom lines). Lines are for zenith angles 60° , 70° , 80° , 87° , and 90° .

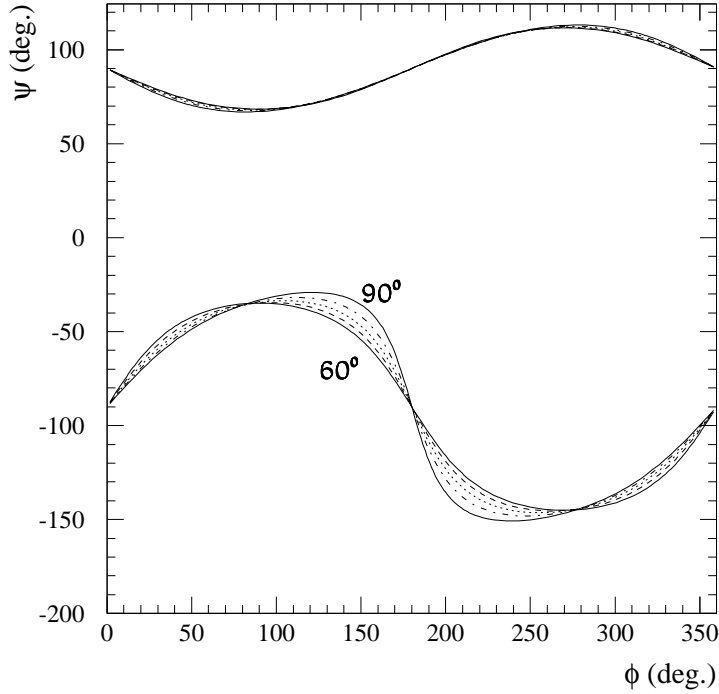


FIG. 6. Angle ψ in the transverse plane (between \vec{B}_\perp and the line parallel to the surface of the Earth, see Fig. 4) as a function of azimuthal angle for the Haverah Park location (top lines) and Pampa Amarilla (bottom lines). Lines are for zenith angle 60° , 70° , 80° , 87° , and 90° .

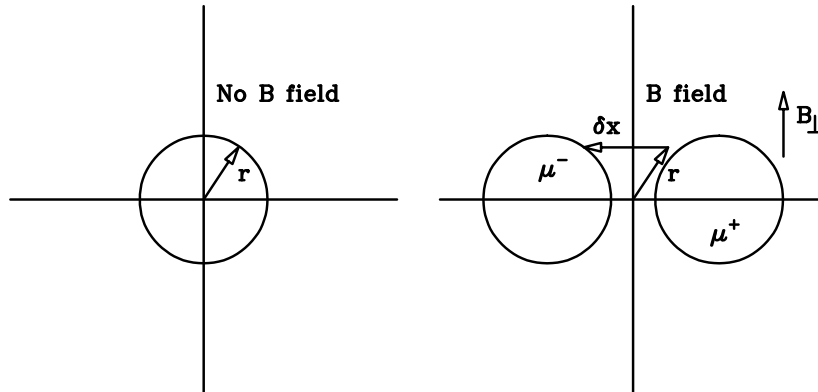


FIG. 7. Toy model composition of deviations due to transverse momentum and to the geomagnetic field. The second graph illustrates how the positive and negative muons that would be a distance r away from shower axis in the absence of magnetic field, are split and deviated an amount δx into two opposite directions along the x axis (perpendicular to \vec{B}_\perp).

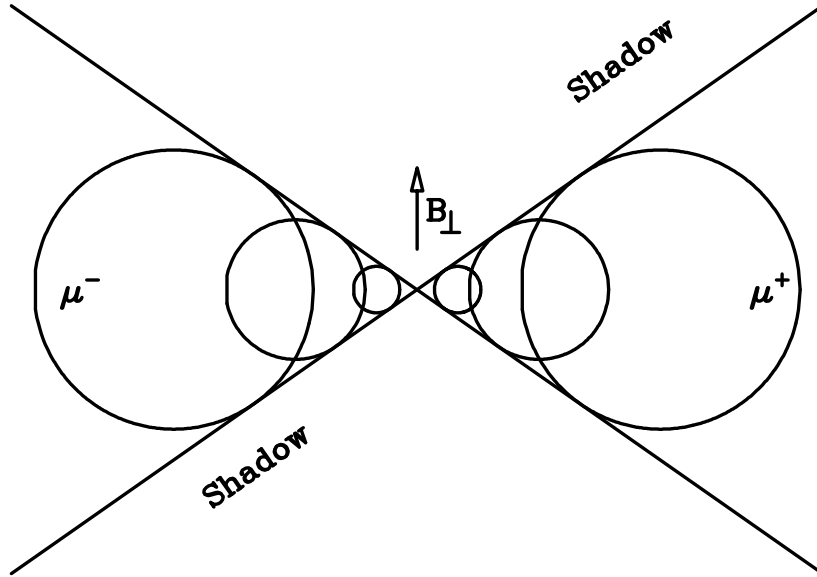


FIG. 8. Toy model magnetic deviations in the transverse plane associated to muons of different energies (and different radii), illustrating the origin of the *shadow* regions in which no muons are expected. The geometrical construction is identical to the two dimensional plot typically used to explain Cherenkov radiation.

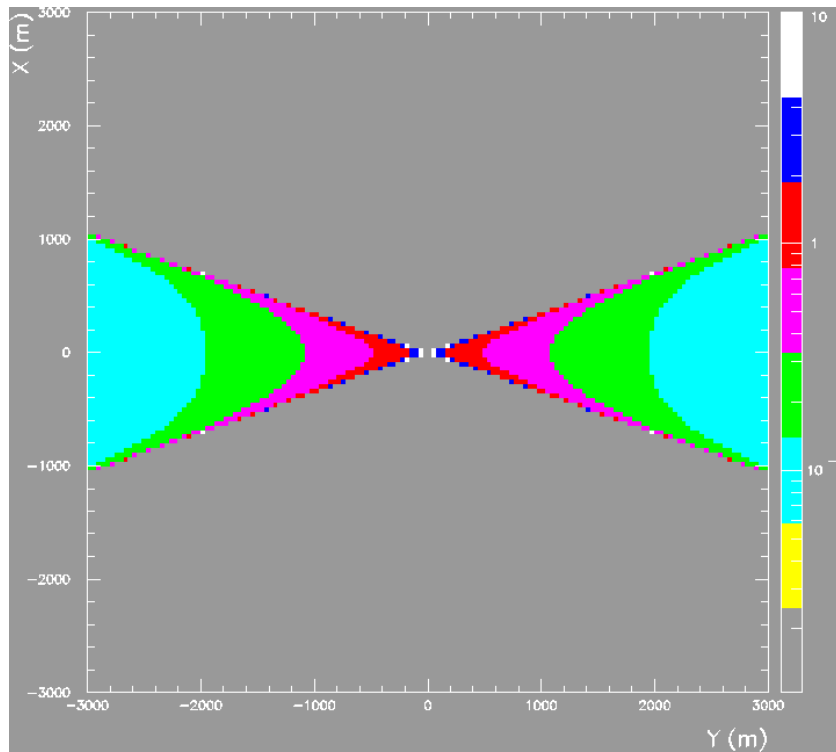


FIG. 9. Toy model results for the muon number densities in the transverse plane with shadow regions as described in the text.

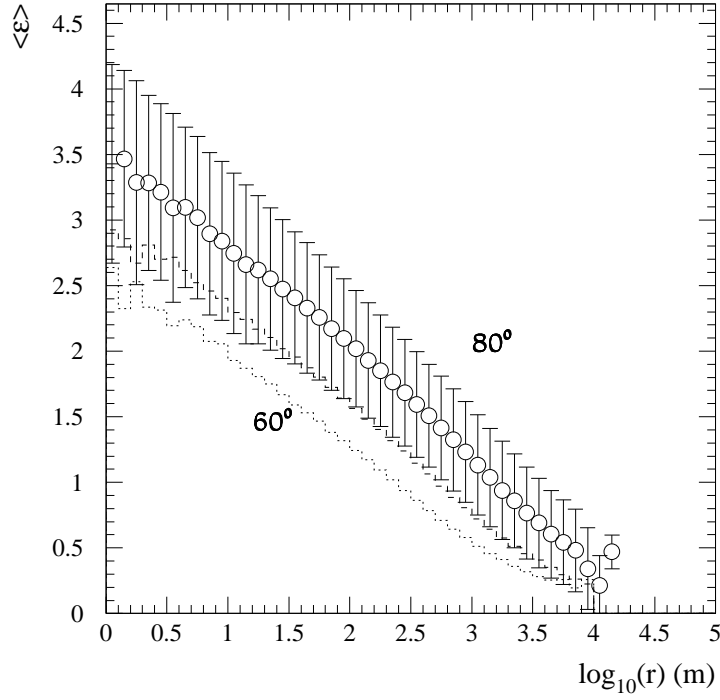


FIG. 10. Correlation between $\langle \epsilon \rangle = \langle \log_{10} E_{\mu} \rangle$ and $\log_{10} r$ for zenith angles 60° , 70° , and 80° from bottom to top, see text. Error bars show the width of the ϵ distribution for 80° .

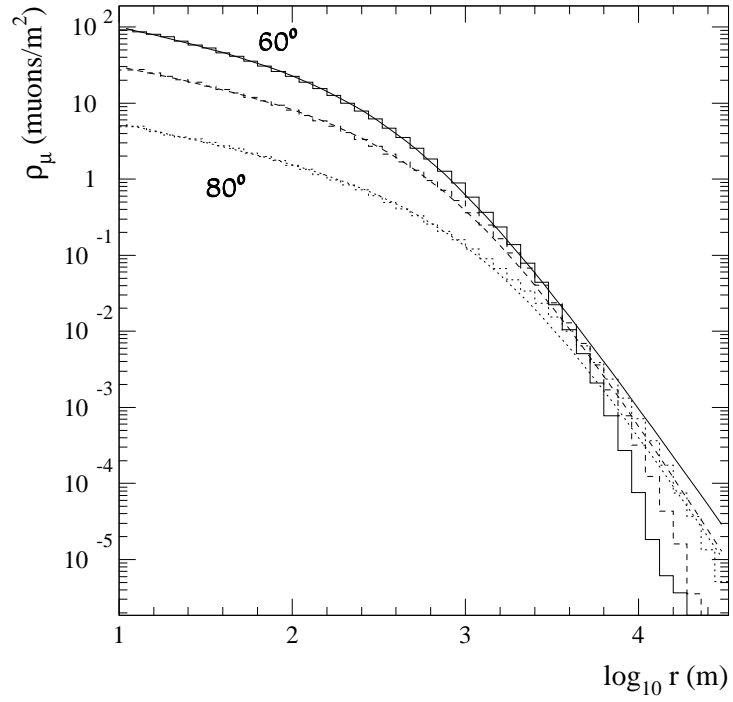


FIG. 11. Lateral distribution of muons as obtained in the simulation and the fit given by Eq. 13. Figures correspond from top to bottom to zenith angles 60° , 70° , and 80° .

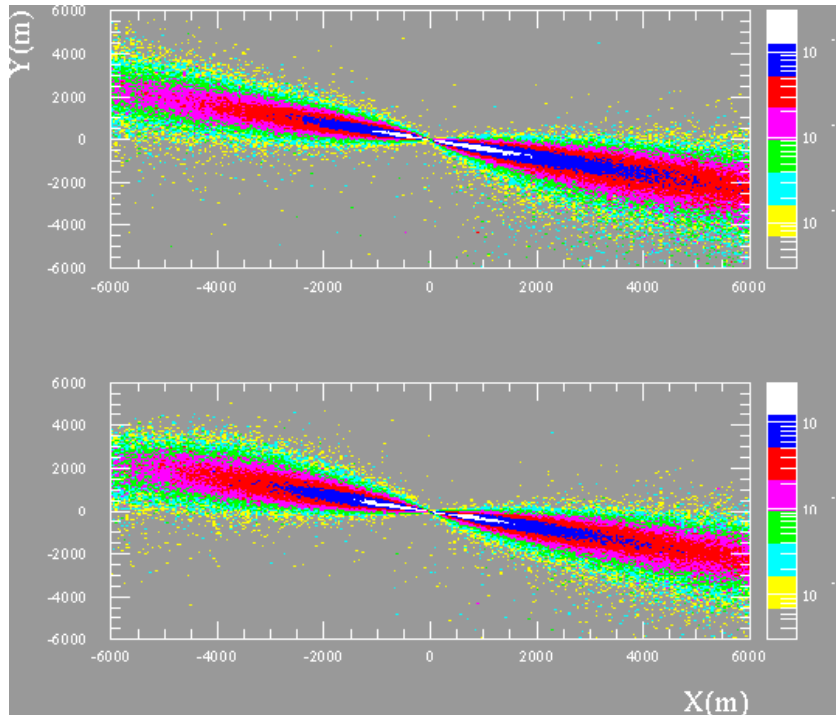


FIG. 12. Muon number density contour plots for $\phi = 90^\circ$ and $\theta = 87^\circ$ using rectangular projection and bulk geometrical correction as described in the text.

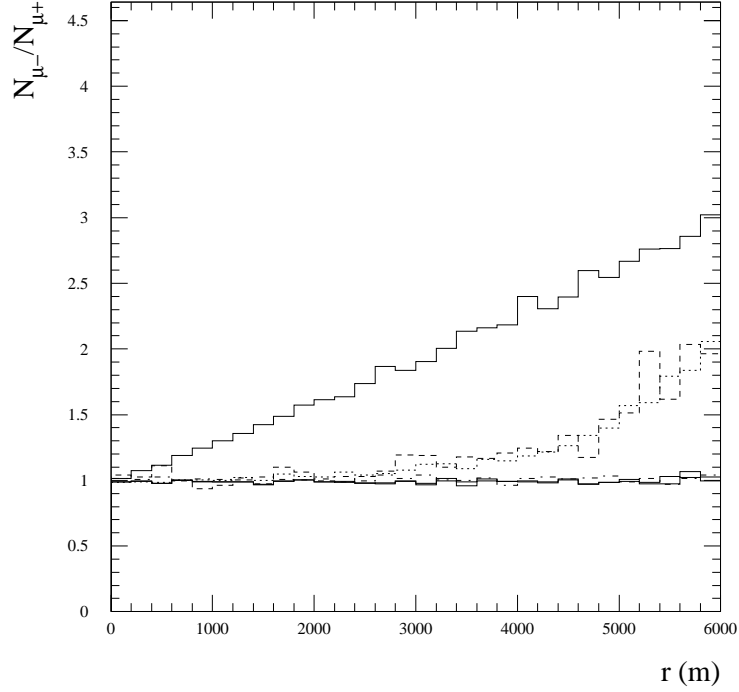


FIG. 13. $\mu^+ \mu^-$ ratio as a function of distance to the core r in the transverse plane for $\phi = 0^\circ$ (bottom lines) and for $\phi = 90^\circ$ (upper lines) using rectangular projection (continuous lines), individual muon extrapolation (dashed lines), and bulk geometrical correction (dotted lines), as described in the text.

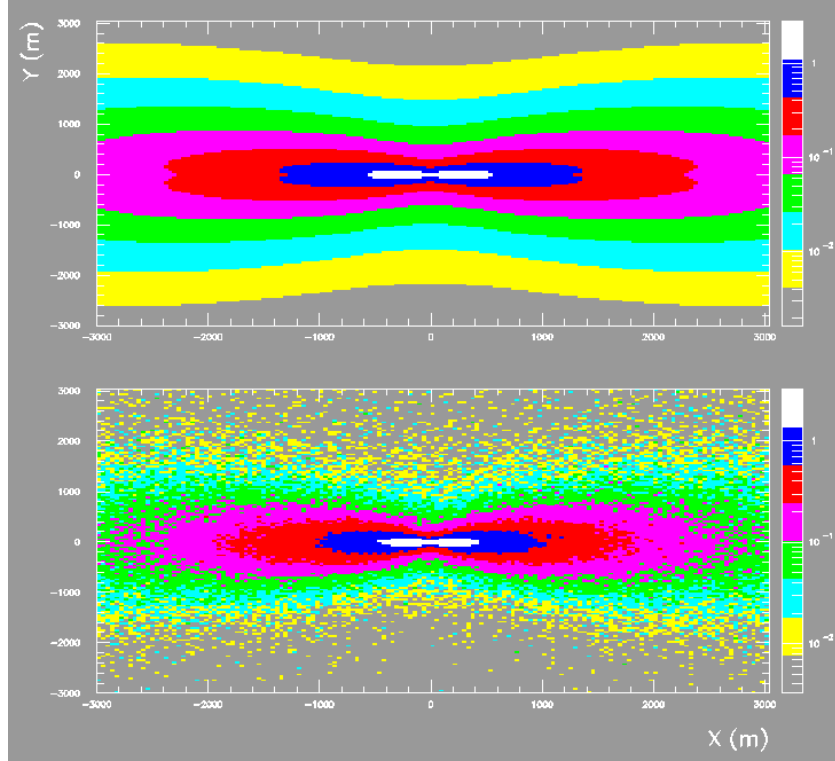


FIG. 14. Contour plots of the muon density in the transverse plane for 10^{19} eV proton showers with an incident zenith angle of 80° as obtained in the simulation for $\phi = 0^\circ$ (lower panel) and in the model (upper panel).

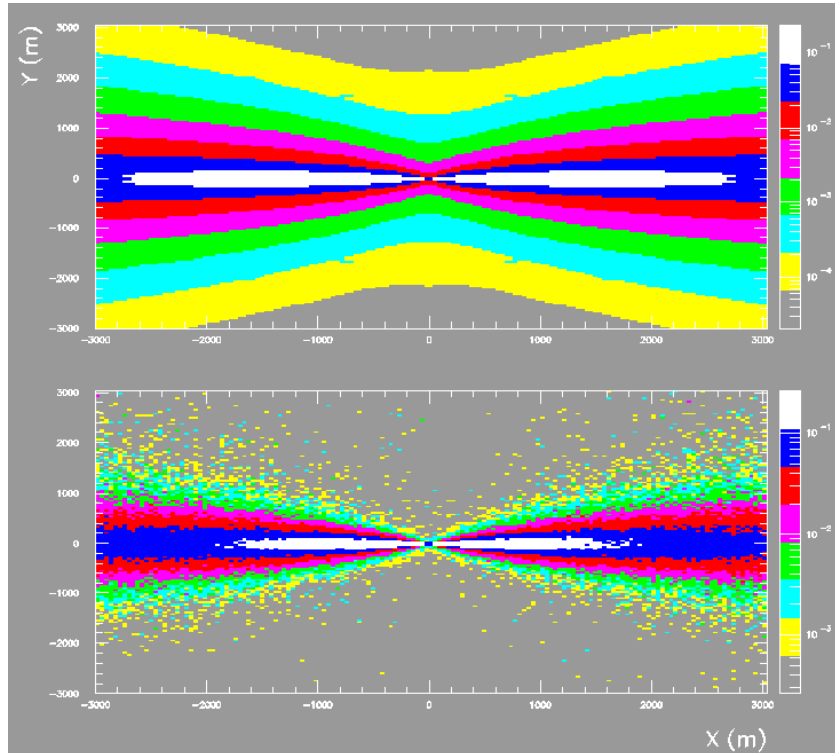


FIG. 15. Same as figure 14 but for incident zenith angle of 87° .

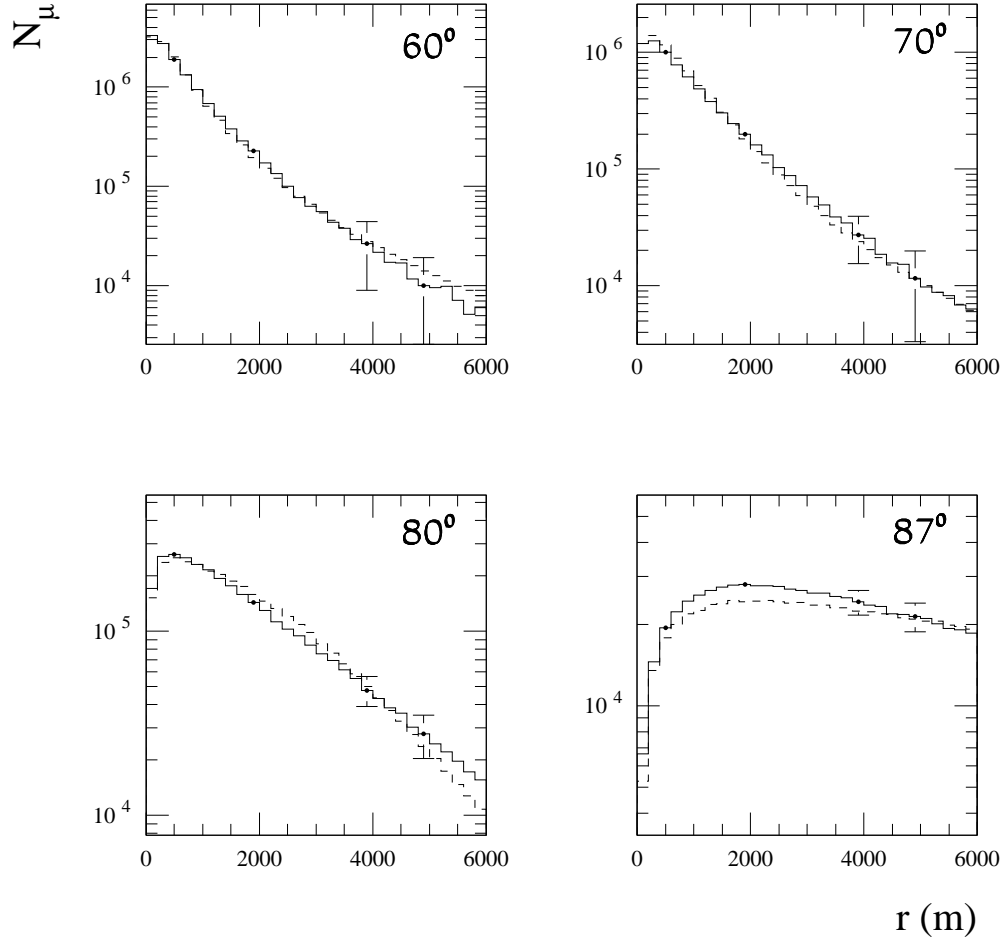


FIG. 16. Transverse distance (r) distributions of the muons in the transverse plane obtained with 10^{19} eV proton shower simulations (continuous histograms) compared to the model (dashed lines) for zenith angles 60° , 70° , 80° , 87° . The error bars shown include both the statistical error and the shower to shower fluctuations.

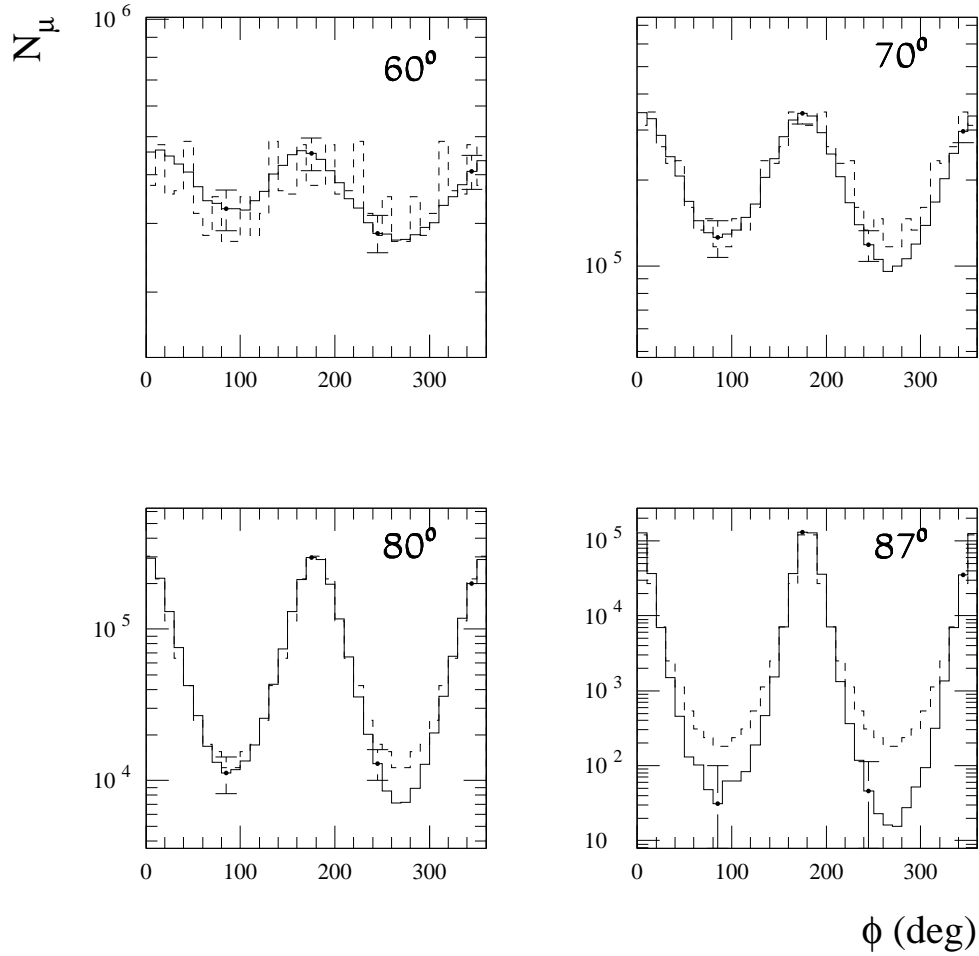


FIG. 17. Azimuthal angle distribution of muons in the transverse plane (integrated up to $r = 6$ km) as obtained in 10^{19} eV proton shower simulations (continuous histogram) compared to the model (dashed histogram) for zenith angles 60° , 70° , 80° , and 87° .

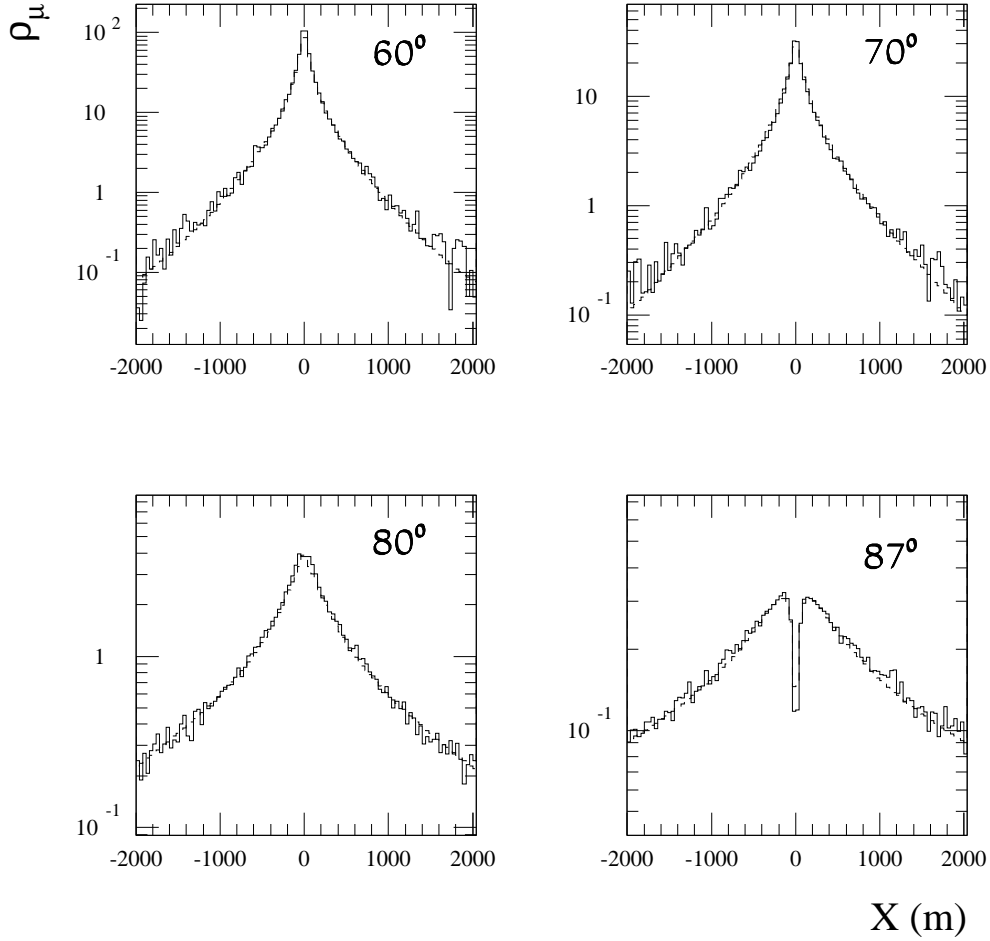


FIG. 18. Muon number density in the transverse plane as a function of the x coordinate for a fixed value of y as obtained in 10^{19} eV proton showers simulations (continuous lines) for $\phi = 0^\circ$ compared to the model (dashed lines). Densities are calculated in 40×40 m bins and the x bins shown are centered at $y = 0$. The figures correspond to zenith angles 60° , 70° , 80° , and 87° .

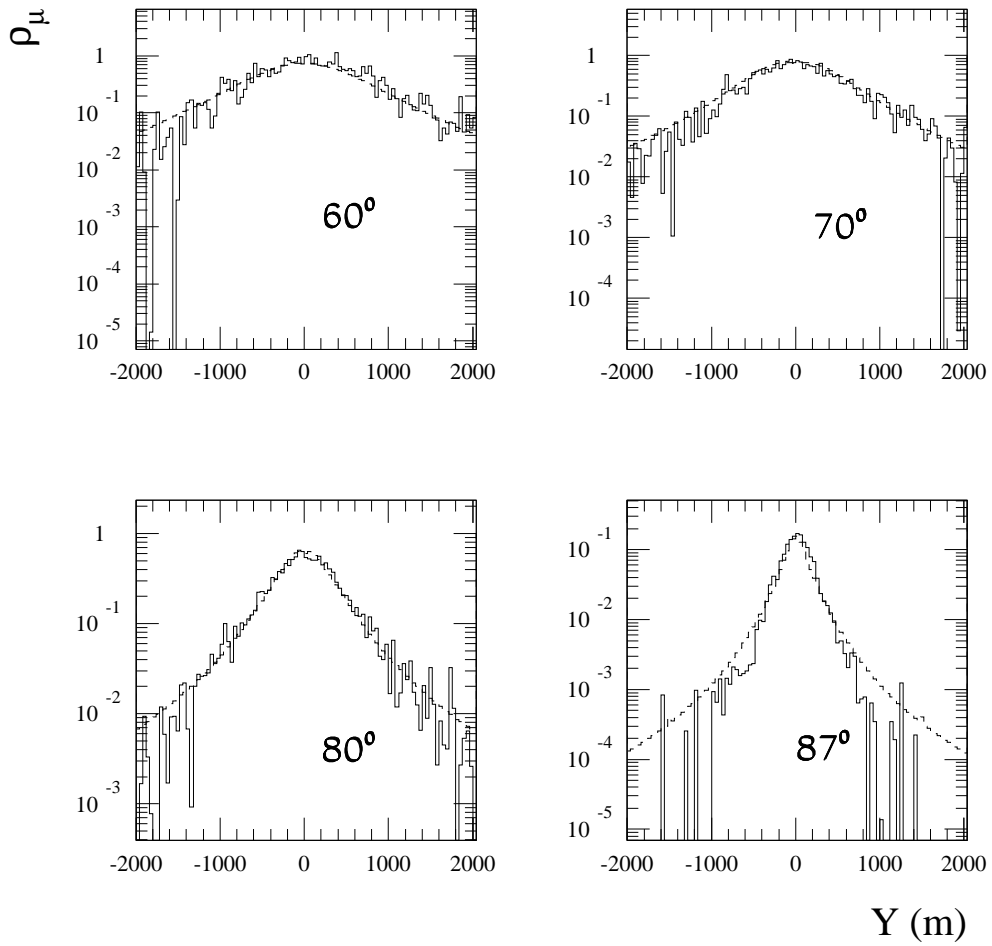


FIG. 19. Same as figure 18 but plotting densities as a function of y at fixed x . Densities shown correspond to y bins centered at $x = 1000$ m.